Potential Flow around Axisymmetric Bodies: Direct and Inverse Problems

M. Fouad Zedan* and Charles Dalton†
University of Houston, Houston, Texas

The direct and inverse problems of incompressible potential flow around an axisymmetric body are solved using an axial source distribution. The source strength is taken to be linearly varying over each element length. A number of examples of representative body shapes have been chosen to represent the method. A comprehensive comparison has been made to the von Kármán method (constant strength element) for the direct method and to earlier results of the authors for the inverse problem. The solutions obtained herein are more stable and accurate, converged faster, and did not require double-precision computation as compared to the constant strength element methods. Compared to the surface singularity method, the present direct problem solution is much simpler and requires less storage and computation time with comparable accuracy for many body shapes. Compared to Bristow's surface-singularity inverse solution, the present solution is again simpler, requires less storage, and converges much faster with fewer calculations in each iteration. A disadvantage is that the present method cannot handle body shapes with sudden changes in the slope of the meridian line.

I. Introduction

THE flow around a body of revolution is, in general, highly complex. The flowfield typically consists of a boundary layer near the body surface, an irrotational region outside the boundary layer, and a wake or separated region aft of the body. For a streamlined body as compared to a bluff body, the complexity of the flowfield is substantially reduced; however, it is still computationally difficult. The viscous resistance to these bodies is usually calculated from the boundary-layer solution, which requires the knowledge of the velocity distribution outside the boundary layer. This velocity distribution is obtained from the potential flow solution. Numerous experimental results have shown that these velocity distributions are in good agreement with measurements outside the boundary layer for nonseparating flow (see Hess and Smith[1]).

In potential flow around bodies, there are two main problems: the direct and the inverse problems. In the direct problem, the body shape is specified and the velocity distribution is required. For the inverse problem, the surface velocity distribution is given while the corresponding body contour is to be calculated. Available solutions to these two problems are either simple, but inaccurate, and limited to simple body shapes (axial singularity distribution methods); or complicated and numerically involved, but accurate for most applications (surface singularity methods). Our objective here is to improve the accuracy and extend the range of applications of the simple class of methods for axisymmetric bodies.

II. Previous Studies

The flow around an axisymmetric body was solved many years ago by von Kármán[2] using an axial distribution of source/sink elements of constant strength. Hereafter, this solution to the direct problem will be referred to as the "von Kármán method." This method has been studied extensively by Oberkampf and Watson.[3] The study showed that the method produces a system of linear equations which is, in general, ill-conditioned, and requires very high computational accuracy (25_{10} significant figures) in the construction of the coefficient matrix and in solving the equations. Oberkampf and Watson concluded that the method does not always produce reliable solutions for the flow around a specified body, and that the conditions that the body should meet in order to be represented by a system of axial line sources are not clear. Karamcheti[4] states that the body should be slender and should not have any discontinuity in the slope of the meridian line. Numerical experiments by Oberkampf and Watson showed that such conditions are not sufficient. For example, the method gave a slight rippling in the velocity distribution as well as in the meridian streamline ($\psi = 0$) of very slender Rankine ovals [*FR* (fineness ratio) = 10)]. Oberkampf and Watson explained the effect to be due to the increased local effects of each source element. Another result of their study is that the method is sensitive not only to the shape of the contour but also to the number of elements used to generate the body.

Another approach to solving the direct problem for bodies of revolution is the surface singularity distribution. This approach is equivalent to the solution of an integral equation of the second kind, which has the advantage that a solution always exists. This approach has received considerable attention recently from various investigators. The most widely used surface singularity method is the surface source density method developed at the Douglas Aircraft Company. The body surface is divided generally into a finite number of elements which are not necessarily equal in size. The source or sink strength is taken as constant over each element. The integral equation can then be transformed into a system of linear algebraic equations. Using this approach, Smith and Pierce[5] developed an exact general method for calculating the flow about or within bodies of almost any shape, provided the flow is either planar or axisymmetric. Hess and Smith[1] summarized the numerous extensions to the method that were developed through 1965 and compared them with experimental results as well as with exact analytic solutions. Even the flow around complicated three-dimensional bodies has been solved, using the same approach, by Hess,[6,7] Webster,[8] and Grodtkjaer.[9] It has been shown by many investigators that the surface singularity methods are more accurate than the axial source/sink distribution method which may not converge for some boundary shapes. However, the

Received July 12, 1977; revision received Nov. 15, 1977.

Index categories: Aerodynamics; Lighter-than-Airships; Hydrodynamics.

*Instructor, Department of Mechanical Engineering. Member AIAA.

†Associate Professor, Department of Mechanical Engineering. Member AIAA.

computational labor in the axial source distribution method is a fraction of that of the surface singularity methods.

For the inverse problem, solutions are not as developed as for the direct problem. The solution of the inverse problem is generally more difficult since it involves the solution of a free boundary value problem. However, it is more important in the design of aero/hydrodynamic shapes, since one can input a velocity distribution that is known to have desirable features for certain applications and then obtain the corresponding body. At the present time, solutions of the inverse problem are limited to two-dimensional and axisymmetric bodies. Hess[10] used the inverse problem to develop what are known as "cavitation shapes," i.e. axisymmetric bodies which have a maximum velocity as small as possible over a very large portion of the body length. Young and Owen[11] and McNown and Hsu[12] developed solutions which are applicable to slender bodies of revolution only. Marshall[13] solved what he defined as the development problem, which is a subproblem in the inverse problem. Only recently, successful methods were developed by Bristow[14] and by Zedan and Dalton[15] for bodies of revolution which are not slender. Bristow solved the inverse problem by iterative use of the Douglas-Neumann direct method, which employs a surface-singularity distribution. He presented three test cases and a very good degree of accuracy was attained in ten iterations. Zedan and Dalton developed a method which employs the axial source/sink distribution, with constant element strength, to obtain a simple solution for the inverse problem. Examples presented show that the method is accurate and converges fast (four iterations) with much less calculation required in each iteration than in Bristow's method. However, the method is limited to bodies that do not have sudden changes in the slope of the meridian line. Hereafter, this method will be referred to as ZD1.

In view of the simplicity of the axial source distribution methods as compared to the surface singularity distribution, and the tremendous saving in memory storage and the amount of numerical calculation, it was considered justifiable to try to improve the accuracy and reduce the limitations of the former class of methods for both the direct and inverse problems. In this study, the improvement is achieved by allowing the source intensity to vary linearly over the element length instead of being constant as in the von Kármán and ZD1 methods.

III. Mathematical Description

In this section, the basic equations for an axial distribution of line sources combined with uniform flow are derived. The strength of each of these elements is allowed to vary linearly along the element. The values of these strengths are continuous at the junction points between each two neighboring elements.

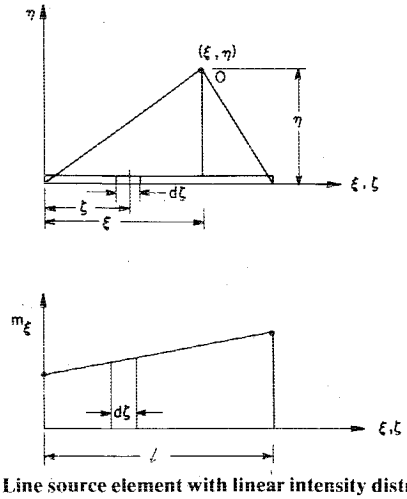

Fig. 1 Line source element with linear intensity distribution.

Equations for an Element

Consider first an element of length ℓ with a variable intensity distribution as shown in Fig. 1. The stream function of this element at a point (ξ,η) is given by[16]

$$\psi=\frac{-1}{4\pi}\int_0^\ell \frac{m_\zeta(\xi-\zeta)\,d\zeta}{\sqrt{(\xi-\zeta)^2+\eta^2}} \tag{1}$$

where m_ζ is the variable intensity along the source element. The induced velocity components at the point (ξ,η) due to this source element can be obtained by applying the equations

$$u=\frac{1}{\eta}\frac{\partial\psi}{\partial\eta} \quad \text{and} \quad v=\frac{-1}{\eta}\frac{\partial\psi}{\partial\xi}$$

Since the integration in Eq. (1) is with respect to ζ, differentiation with respect to η and ξ can be applied to the integrand. This leads to

$$u=\frac{1}{4\pi}\int_0^\ell \frac{m_\zeta(\xi-\zeta)}{[(\xi-\zeta)^2+\eta^2]^{3/2}}\,d\zeta \tag{2}$$

and

$$v=\frac{1}{4\pi\eta}\int_0^\ell m_\zeta\left[\frac{1}{\sqrt{(\xi-\zeta)^2+\eta^2}}-\frac{(\xi-\zeta)^2}{[(\xi-\zeta)^2+\eta^2]^{3/2}}\right]d\zeta \tag{3}$$

The linear variation of the source intensity m_ζ is represented by

$$m_\zeta=\alpha+\beta\zeta \tag{4}$$

where α and β are constants to be determined later.

Substituting for m_ζ in Eqs. (1-3), from Eq. (4), the three integrals can be evaluated in closed form. The results will be in terms of the constants α and β as expected,

$$\psi(\xi,\eta)=1/4\pi[\alpha(H_2-\xi H_1)+\beta(H_3-\xi H_2)] \tag{5}$$

$$u(\xi,\eta)=1/4\pi[\alpha(\xi P_1-P_2)+\beta(\xi P_2-P_3)] \tag{6}$$

and

$$v(\xi,\eta)=1/4\pi\eta[\alpha(H_1-\xi^2P_1+2\xi P_2-P_3)+\beta(H_2-\xi^2P_2+2\xi P_3-P_4)] \tag{7}$$

where $H_1,\ldots H_3$ and $P_1,\ldots P_4$ are functions of ξ and η. These functions are described by the following integrals,

$$H_k(\xi,\eta)=\int_0^\ell \frac{\zeta^{k-1}}{\sqrt{(\xi-\zeta)^2+\eta^2}}\,d\zeta \tag{8}$$

and

$$P_k(\xi,\eta)=\int_0^\ell \frac{\zeta^{k-1}}{[(\xi-\zeta)^2+\eta^2]^{3/2}}\,d\zeta \tag{9}$$

The closed form results of the above integrals for various values of k are

$$H_1(\xi,\eta)=\ln\left(\frac{F_1+\ell-\xi}{F_2-\xi}\right) \tag{10a}$$

$$H_2(\xi,\eta)=F_1-F_2+\xi H_1 \tag{10b}$$

$$H_3(\xi,\eta)=\tfrac{1}{2}[(\ell+3\xi)F_1-3\xi F_2+(2\xi^2-\eta^2)H_1] \tag{10c}$$

$$P_1(\xi,\eta)=\frac{\ell-\xi}{\eta^2 F_1}+\frac{\xi}{\eta^2 F_2} \tag{11a}$$

$$P_2(\xi,\eta)=\frac{\xi\ell-(\xi^2+\eta^2)}{\eta^2 F_1}+\frac{F_2}{\eta^2} \tag{11b}$$

$$P_3(\xi,\eta)=\frac{(\xi^2-\eta^2)\ell-\xi(\xi^2+\eta^2)}{\eta^2 F_1}+\frac{\xi}{\eta^2}F_2+H_1 \tag{11c}$$

and

$$P_4(\xi,\eta)=\frac{\ell^2}{F_1}+3\xi P_3-2(\xi^2+\eta^2)P_2 \tag{11d}$$

where

$$F_1=\sqrt{\ell^2-2\xi\ell+\xi^2+\eta^2} \text{ and } F_2=\sqrt{\xi^2+\eta^2}$$

Equations for Axial Source Distribution in Uniform Flow

The distribution considered here will be in the form of elements along the axis of symmetry of the body as shown in Fig. 2. Also shown is the strength distribution $m(\xi)$, which is approximated by a straight line segment over each element with no discontinuities at junction points between elements. Our objective here is to derive expressions for the stream function and the velocity components for such a distribution in a uniform stream.

Consider the jth element. Since values of m are continuous at junction points, then the coefficients α and β that appear in Eq. (4) are

$$\alpha=\sigma_j$$

and

$$\beta=(\sigma_{j+1}-\sigma_j)/\ell_j \tag{12}$$

where σ_j is the value of m at the junction point between elements j and $j-1$. Substituting into Eqs. (5-7), we obtain the ψ, u, and v contributions due to an element j at a control point i as follows:

$$\psi_j=1/4\pi\,[\sigma_j a_{ij}+\sigma_{j+1}b_{ij}] \tag{13a}$$

$$u_j=1/4\pi\,[\sigma_j c_{ij}+\sigma_{j+1}d_{ij}] \tag{13b}$$

$$v_j=1/4\pi r_i\,[\sigma_j e_{ij}+\sigma_{j+1}f_{ij}] \tag{13c}$$

The matrices $a_{ij}, b_{ij}, \ldots f_{ij}$ are given by

$$a_{ij}=H_2-\xi H_1-b_{ij} \tag{14a}$$

$$b_{ij}=(H_3-\xi H_2)/\ell_j \tag{14b}$$

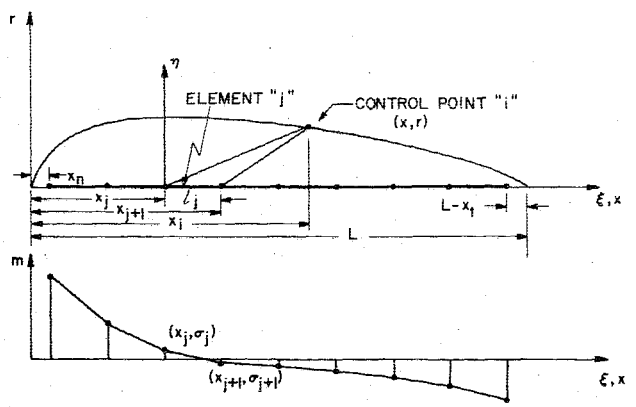

Fig. 2 Geometry of the body and the singularity distribution along the axis.

$$c_{ij}=\xi P_1-P_2-d_{ij} \tag{14c}$$

$$d_{ij}=(\xi P_2-P_3)/\ell_j \tag{14d}$$

$$e_{ij}=H_1-\xi^2 P_1+2\xi P_2-f_{ij} \tag{14e}$$

and

$$f_{ij}=(H_2-\xi^2 P_2+2\xi P_3-P_4)/\ell_j \tag{14f}$$

where the functions $H_1,\ldots H_3$ and $P_1,P_2,\ldots P_4$ are to be calculated using the Eqs. (10) and (11) with

$$\xi=x_i-x_j \text{ and } \eta=r_i \tag{15}$$

Adding the contributions due to N elements and the uniform flow, the total stream function at a control point i becomes

$$\psi_i=\frac{1}{4\pi}\sum_{j=1}^{N}(\sigma_j a_{ij}+\sigma_{j+1}b_{ij})+U_\infty\frac{r_i^2}{2}$$

Expanding the summation term and rearranging the terms, one obtains

$$\psi_i=\frac{1}{4\pi}\sum_{j=1}^{N+1}\sigma_j(a_{ij}+b_{i,j-1})+U_\infty\frac{r_i^2}{2} \tag{16}$$

with

$$b_{i,0}=0 \text{ and } a_{i,N+1}=0$$

In a similar fashion, the corresponding expressions for the velocity components are

$$u_i=\frac{1}{4\pi}\sum_{j=1}^{N+1}\sigma_j(c_{ij}+d_{i,j-1})+U_\infty \tag{17}$$

and

$$v_i=\frac{1}{4\pi r_i}\sum_{j=1}^{N+1}\sigma_j(e_{ij}+f_{i,j-1}) \tag{18}$$

with $d_{i,0}$, $c_{i,N+1}$, $f_{i,0}$, and $e_{i,N+1}$ as zeros.

Using U_∞ as a reference velocity and ℓ_s as a reference length, Eqs. (16-18) can be put in almost the same dimensionless form used in ZD1,

$$\Psi_i=\frac{1}{4\pi}\sum_{j=1}^{N+1}\bar{\Psi}_{ij}\mu_j+R_i^2/2 \tag{19}$$

$$U_i=\frac{1}{4\pi}\sum_{j=1}^{N+1}\bar{U}_{ij}\mu_j+1 \tag{20}$$

and

$$V_i=\frac{1}{4\pi R_i}\sum_{j=1}^{N+1}\bar{V}_{ij}\mu_j \tag{21}$$

where

$$R_i=r_{i/\ell_s},\quad \mu_j=\sigma_{j/U_\infty\ell_s},\quad \Psi_i=\psi_{i/U_\infty\ell_s^2}$$

$$\bar{\Psi}_{ij}=(a_{ij}+b_{i,j-1})/\ell_s$$

$$\bar{U}_{ij}=\ell_s(c_{ij}+d_{i,j-1})$$

and

$$\bar{V}_{ij}=(e_{ij}+f_{i,j-1})$$

(ℓ_s will be identified later either as the body axial length L or the element length ℓ.)

It should be remembered that the matrices $\bar{\Psi}_{ij}$, $\bar{U}_{ij}$, and $\bar{V}_{ij}$ are functions of the body geometry only, and μ_j is the dimensionless value of the source intensity σ_j at the junction point between elements j and $j-1$.

Tangency Condition

Since the total velocity is everywhere tangential to the body surface in potential flow, it follows that the ratio of V/U is equal to the slope of the meridian streamline (body contour),

$$\left(\frac{dR}{dX}\right)_i = V_i/U_i \tag{22}$$

It could be shown that this condition is equivalent to Eq. (19) when equating Ψ_i to a constant on the body surface. Zedan and Dalton[15] utilized these two equivalent conditions to solve the inverse problem iteratively. The same idea will be used in this paper also.

Closure Condition

For closed profiles, the net efflux of the source/sink elements should be zero. Mathematically, this is equivalent to

$$\sum_{j=1}^{N} \bar{Q}_j = 0 \tag{23}$$

For element j,

$$\bar{Q}_j = \int_0^{\ell_j} m_\xi d_\xi - \frac{\ell_j}{2}(\sigma_j + \sigma_{j+1})$$

Substituting into Eq. (23) and after some algebraic manipulation, one obtains

$$\sum_{j=1}^{N+1} \mu_j \left(\frac{\ell_j + \ell_{j-1}}{\ell_s}\right) = 0 \tag{24}$$

with ℓ_0 and ℓ_{N+1} as zeros.

IV. Solution of Direct Problem

As mentioned previously, the von Kármán method used source/sink elements of constant strength to represent the body. By equating ψ_i at a number of control points on the body surface equal to the number of elements to zero, the following linear system of equations is obtained,

$$\sum_{j=1}^{N} \bar{\Psi}_{ij} M_j = -R_i^2/2 \tag{25}$$

The dimensionless source strengths M_j are calculated by solving this system of equations. The velocity components are obtained by substituting M_j into expressions similar to Eqs. (20) and (21). These expressions as well as $\bar{\Psi}_{ij}$, $\bar{U}_{ij}$, and $\bar{V}_{ij}$ are given in ZD1.

A similar procedure is used in the present scheme to solve the direct problem. With $\Psi_i = 0$ at N control points, Eq. (19) yields a system of N linear algebraic equations in $(N+1)$ unknowns. The closure condition represented by Eq. (24) is used to complete the system. Solving these linear equations yields the values of the source intensities μ_j at the junction points. The velocity components U_i and V_i are calculated by substituting μ_j into Eqs. (20) and (21).

In order to gain a better understanding of the computational problems, a preliminary investigation was performed to compare the von Kármán method and the present scheme. The calculations were done on a UNIVAC 1108 computer. The sphere represented the test case.

When the coordinates were normalized by the body axial length L, the von Kármán method gave good results, except near the stagnation points, in single and double precision for $N = 10$ and 12; the solution blew up at $N = 11$, 20, and higher. Normalizing the coordinates by the element length ℓ, which is equivalent to the Oberkampf and Watson[3] calculations, improved the solution substantially for $N = 12$, 18, and 20, while the solution was again incorrect for $N = 30$ and all odd values. The difficulty can be explained by considering the elements of the coefficient matrix of the system of equations ψ_{ij},

$$\psi_{ij} = \sqrt{(x_i - x_j - \ell_j)^2 + r_i^2} - \sqrt{(x_i - x_j)^2 + r_i^2}$$

For small ℓ_j, two quantities of almost equal value are subtracted, which results in a potentially dangerous loss of significance.[17] This explains why the accuracy decreases as the number of elements increases. On the other hand, using a small number of elements means a smaller number of control points which may not be sufficient to define the body shape well. Using L to normalize the coordinates reduces the absolute value of the two square roots and thus increases the relative round off error, while using the element length ℓ has an opposite effect.

A similar investigation was carried out on the present scheme. Normalization by either L or ℓ produced very little difference. Very accurate results, except very near the stagnation points, were obtained for all values of N as used in the von Kármán method study. The results of the preliminary investigation demonstrated quite well the superiority of the present method over the von Kármán method.

The performances of the two methods are compared by applying them to a number of test cases that have exact solutions. The effect of the number of elements on both methods is also presented. The test cases are Rankine bodies of revolution, airfoil-type axisymmetric bodies of different fineness ratio, and the minimum drag body developed recently by Parsons et al.[18] Results of preliminary test cases showed that double-precision calculations are essential in the case of the von Kármán method and single-precision calculations are satisfactory for the present method. Therefore, double-precision calculations were used for the von Kármán method and single-precision ones for the present scheme unless otherwise stated. The element length ℓ was used to normalize coordinates in both methods.

Test Case 1: Flow Past Rankine Bodies of Revolution

The two methods have been used to calculate the velocity distribution around Rankine bodies of FR = 2, 4, and 10, which cover the practical range.

FR = 2

The two methods gave almost identical results in good agreement with the exact solution for 12 and 20 elements,

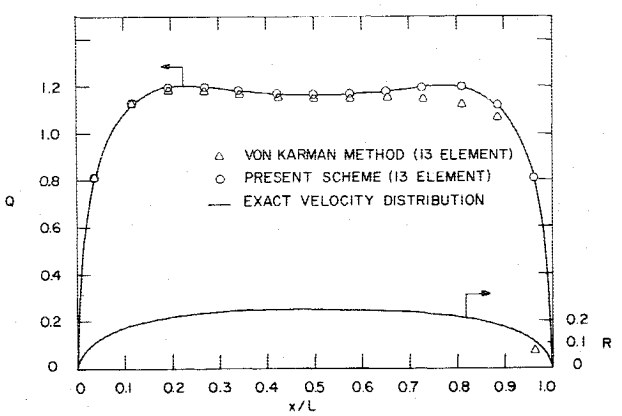

Fig. 3 The velocity distribution for a Rankine body of revolution of FR = 2, calculated by von Kármán method and the present direct problem scheme for 13 elements.

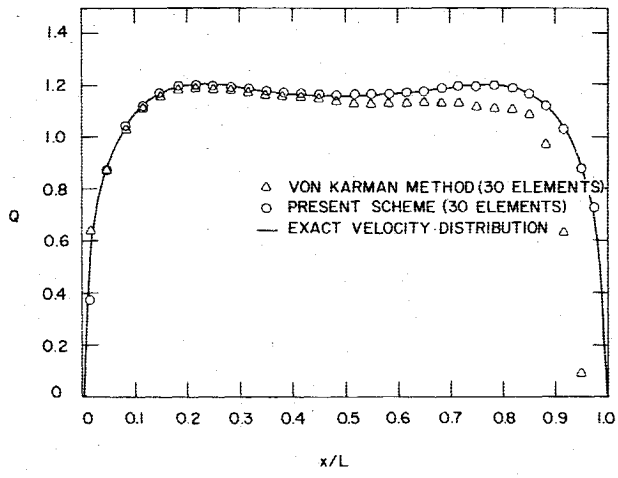

Fig. 4 The velocity distribution for a Rankine body of FR = 2, calculated using 30 elements.

while the present method was more accurate for 13 and 21 elements. Figure 3 shows the velocity distribution obtained by the two methods with 13 elements as compared to the exact solution. The accuracy of the von Kármán method drops sharply as one proceeds toward the trailing stagnation point for $N=30$ and 39. Figure 4 shows a comparison similar to that of Fig. 3 for $N=30$. For $N=31$ and 39 (not shown), the von Kármán method gave completely wrong results everywhere, while the results of the present scheme are still in excellent agreement with the exact velocity distribution.

FR = 4

The two methods have been applied to this case with 12, 13, 20, 21, 30, 31, 38, and 39 elements. For all the even numbers of elements, both methods gave results in excellent agreement with the exact velocity distribution. The von Kármán method gave inaccurate results over the rear 15% of the body length for all the odd numbers of elements, while the present method gave the same degree of accuracy as before.

FR = 10

Similar comparisons were carried out for FR = 10. The two methods gave reasonably accurate results for all even numbers of elements; however, the present method has a slight edge. This becomes clear if one plots the v component of the total velocity as shown in Fig. 5. The present method gives a relatively smooth variation compared to the von Kármán method, which gave fluctuating values. The fluctuations in the v component are inconsistent with the tangency condition since the body meridian contour is smooth. However, the total velocity distribution was not affected by such fluctuations. This is because the magnitude of v is almost negligible in comparison to u over about 75% of the body length for this high fineness ratio. It is worthwile to note that, for this high fineness ratio case, the performance of the von Kármán method for odd numbers of elements was fair compared to its poor performance for odd numbers of elements in the previous two examples. The performance of the present method remained as good as its performance for even numbers of elements.

Test Case 2: Flow Around Airfoil-Type Axisymmetric Bodies

Unlike Rankine bodies, this class of bodies is not symmetrical about the central cross plane. These bodies are generated by adding a point source, a line sink of equal total influx, and a uniform flow. Different fineness ratios are obtained by changing the source strength. The results of the two schemes are compared with the exact solutions for the flow around two bodies of FR ≅ 2.91 and 4.46.

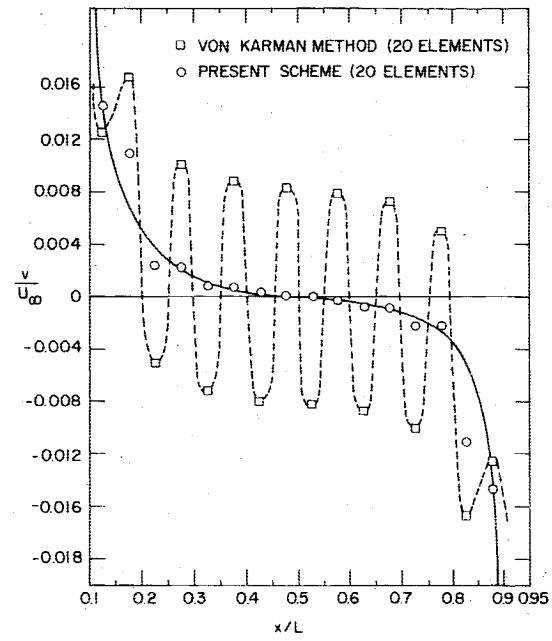

Fig. 5 The radial velcoity component distribution for a Rankine body of FR = 10.

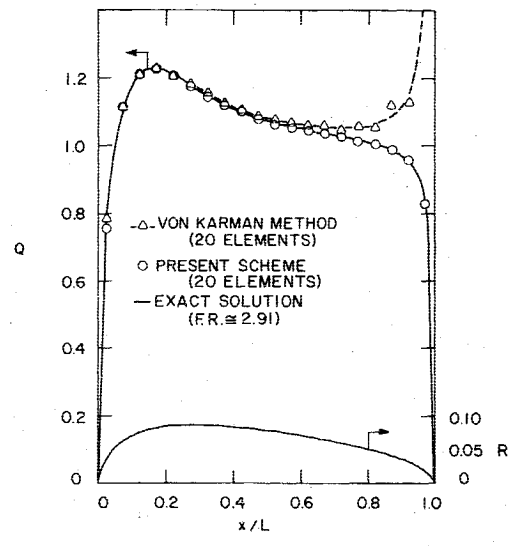

Fig. 6 The velocity distribution and the meridian line for an airfoil-type axisymmetric body of FR ≅ 2.91.

FR ≅ 2.91

Comparison was carried out for different numbers of elements ranging from 10 to 39 as before. The comparison showed that the von Kármán method velocity distribution was erroneous at most numbers of elements. The best performance was at $N=20$; however, the solution started to fail increasingly from the leading to the trailing stagnation points. On the other hand, the present method gave results in consistently excellent agreement with the exact velocity distribution at all values of N. Figure 6 shows a comparison between the results of the two schemes for $N=20$.

FR ≅ 4.46

Similar comparisons to the previous case are carried out here. The present scheme, once again, gave very accurate results at all points and for all values of N, while the velocity distribution obtained by the von Kármán method is generally poor over the rear 10-15% of the body length at all values of N, with the best results at $N=20$. A comparison between the velocity distributions predicted by both schemes for $N=20$

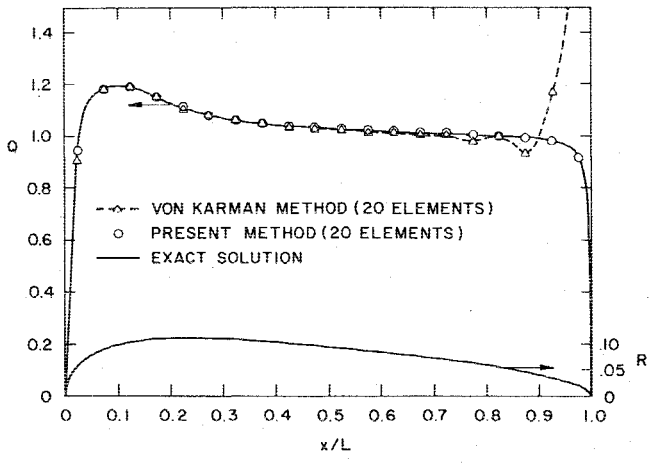

Fig. 7 The velocity distribution and the meridian line for an airfoil-type axisymmetric body of FR ≅ 4.46.

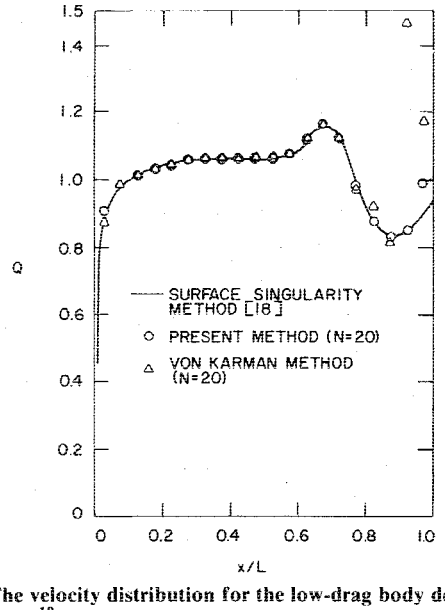

Fig. 8 The velocity distribution for the low-drag body developed by Parsons et al.[18]

and the exact solution is shown in Fig. 7. We also calculated the error in the velocity components u and v, respectively. It is interesting that the von Kármán method gives a reasonably small error in the u component in the range $0.1 \leq x/L \leq 0.6$, but that the error increases sharply and monotonically for $x/L > 0.6$. The present scheme has almost zero error in the range $0.075 \leq x/L \leq 0.925$ and negligibly small error very close to the leading and rear stagnation points. The error in the v component fluctuates for the von Kármán method, but its absolute value is similar to the error in u component for both methods.

Test Case 3: Flow Around a Low Drag Laminar Profile

Parsons et al[18] used the Douglas-Neumann program together with a boundary-layer drag calculation method and a computer-oriented optimization scheme for shaping axisymmetric bodies for minimum drag. Their study resulted in a body which has a drag coefficient one-third less than the best, previously available laminar design. The coordinates of the body meridian contour and the velocity distribution calculated by the Douglas program were given in Ref. 18. The body has a tailboom and an inflection point. Since these features are not present in the previous examples, we decided to use it as another test case.

To deal with tailboom bodies, the closure condition, Eq. (23), should be modified such that

$$\sum_{j=1}^{N} \bar{Q}_j = \pi r_t^2 u_t$$

Thus, Eq. (24) becomes

$$\sum_{j=1}^{N+1} \mu_j \left(\frac{\ell_j + \ell_{j-1}}{\ell_s} \right) = \pi R_t^2 U_t \tag{26}$$

where the subscript t refers to values at the tail. Since U_t is not known in advance, it has been assumed equal to 0.95 as a first estimate. If the calculated velocity distribution gives a value for U_t that is much different, the solution should be repeated in an iterative manner. Our results show that such an iteration is not necessary. Figure 8 shows the velocity distribution obtained by the present scheme with 20 elements as compared to the velocity calculated by the sophisticated surface singularity method as given in Ref. 18. The agreement is excellent everywhere (except at one point) at a fraction of the numerical labor.

The velocity distribution obtained by the von Kármán method with 20 elements is also shown in Fig. 8. Good agreement with the other two solutions is clear in the range $0 \leq X \leq 0.8$, while it diverges badly for $X > 0.8$. The solution is even worse than shown near the trailing edge since the v component of velocity fluctuates between large positive and negative values in this region. Using a larger number of elements produces a more erroneous solution. The present scheme shows much less sensitivity to the number of elements.

This example shows that linear variation of source strength over the elements has led to an axial singularity distribution that can represent bodies of revolution with inflection points, while the constant strength elements failed to represent such bodies accurately. The inadequacy of the constant strength elements for such a case has been reported by Karamcheti[4] and Oberkampf and Watson.[3]

V. Solution of Inverse Problem

The inverse problem (sometimes called the design problem) is formulated as: "Given the surface velocity distribution, what is the body shape that will produce this distribution?" This problem is solved here using essentially the same general approach developed recently by the authors (ZD1). The iterative approach is based on using two equivalent conditions; the tangency condition [Eq. (22)] and a constant value for the stream function on the body surface, together with the usual U and V expressions.

An improved solution is achieved in this paper by using the linear singularity variation over each singularity element, instead of the constant strength elements used in ZD1. For completeness, the method is described briefly here.

Since $Q_i^2 = U_i^2 + V_i^2$, the tangency condition of Eq. (22) is written as

$$U_i = \frac{Q_i}{\sqrt{1 + (\mathrm{d}R/\mathrm{d}X)_i^2}} \tag{27}$$

Equation (20) is rewritten, for convenience, as

$$\frac{1}{4\pi} \sum_{j=1}^{N+1} \bar{U}_{ij} \mu_j = U_i - 1 \tag{28}$$

and, since $\Psi_i = 0$ at the control points, Eq. (19) becomes

$$R_i = \sqrt{\frac{-1}{2\pi} \sum_{j=1}^{N+1} \bar{\Psi}_{ij} \mu_j} \tag{29}$$

The method starts with an initial guess of the body shape R_i^0 (an ellipsoid of high FR has been used in all calculations). The

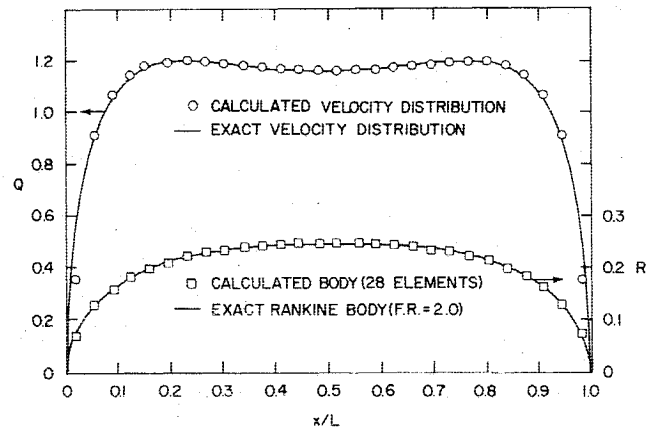

Fig. 9 A comparison between the body geometry and the velocity distribution calculated by the present inverse problem scheme and the exact body and the exact (input) velocity distribution for a Rankine body of FR = 2.

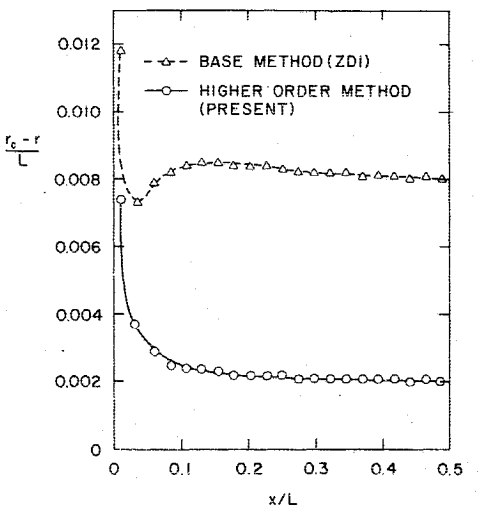

Fig. 10 The error in the radius of the calculated Rankine body of FR = 4, N = 42.

slopes $(dR/dX)_i$ at the control points as well as the matrices $\bar{\Psi}_{ij}$, $\bar{U}_{ij}$, and $\bar{V}_{ij}$ are calculated for this initial geometry from the expressions following Eq. (21). With the slopes just calculated and the prescribed velocity distribution Q_i, the axial velocity component U_i is calculated from Eq. (27). Having calculated U_i and $\bar{U}_{ij}$, the system of linear Eq. (28) is solved by Gaussian elimination to obtain the values μ_j of the singularity distribution at the junction points. The radial velocity component is then calculated from Eq. (21) by substituting the values of μ_j just obtained. This singularity distribution μ_j and the matrix $\bar{\Psi}_{ij}$ are substituted in Eq. (29) to obtain an improved geometry $R_i^{(1)}$. These new body coordinates replace the initial guess $R_i^{(0)}$, and another iteration is executed until convergence is attained. Three convergence criteria were discussed in ZD1. The most practical is to compare the calculated velocity distribution in each iteration with the prescribed one; if they agree, iteration is stopped.

It should be noted that the system of Eq. (28) represents N equations (i.e., N control points) in $(N+1)$ unknowns μ_j. The system is closed by solving the closure condition, Eq. (24), simultaneously with the other equations.

The scheme just described was used to develop a number of body shapes from prescribed velocity distributions. These velocity distributions were chosen for bodies which have exact solutions. The calculated body shapes were compared to the exact bodies to evaluate the accuracy and the limitations of the method. Comparison is also made with the corresponding results of the previous method (ZD1).

Test Case 1: Ranking Bodies of Revolution

The present inverse problem method has been used to develop Rankine bodies of FR = 2, 4, and 10 from the corresponding analytic velocity distributions. In each case, the developed body and the velocity calculated in the convergence iteration are compared to the exact body and velocity distribution respectively.

FR = 2

Using 20 elements for a Rankine body of FR = 2, the solution converged after four iterations. Figure 9 shows the converged body and the exact body as well as the prescribed (exact) and the calculated velocity distribution. The agreements between the calculated (after four iterations) and the exact body, and between the calculated and prescribed velocity distribution, are quite good.

Since the same test case had been used in ZD1, we show the improvement brought by present scheme by comparing the error in body shape developed by both schemes for the same number of elements. The present method has less error at all points particularly near the front and rear stagnation points. Not only this, but also the accuracy of the present method was negligibly affected by the use of the single-precision calculations, unlike the base method ZD1 for which double-precision calculations were necessary.

FR = 4

The results of the two schemes were compared for FR = 4. Forty-two elements were used for each method and convergence was attained in four iterations in both cases. The error in the calculated body contour is plotted in Fig. 10. The present method has much less error everywhere as compared to the results of ZD1; however, both methods are less accurate near the leading and trailing stagnation points as compared to the midpart of the body.

FR = 10

A similar comparison of the results for this case show that both methods give the same degree of accuracy in the calculation of the body contour. However, the velocity calculated from the singularity distribution in the convergence iteration (iteration four for both methods) is in slightly better agreement with the input velocity distribution for the present scheme. The method of ZD1 produced a fluctuating ratio of V/U, whereas the present method yielded a smooth distribution in agreement with dR/dX as shown in Fig. 11. The lack of smoothness of the ZD1 results indicates some incompatibility between the calculated and given velocity distributions. However, one should remember that the effects of such oscillations on the calculated velocity near the middle of the body are negligible since the magnitude of the V component is very small in this region for such a slender body.

Test Case 2: Airfoil-Type Body of Revolution

This case of bodies was used before as a test case for the direct problem solution here and the inverse problem base method (ZD1). The present higher order solution for the inverse problem has been applied to the two fineness ratios used in ZD1 and with the same number of elements in order to make a meaningful comparison.

FR ≅ 2.91

The solution converged after four iterations for 36 elements. Comparison with the corresponding results from ZD1 is accomplished by calculating the error in the calculated profile in both cases. Figure 12 shows that the error produced by the present scheme is everywhere less than that produced by the base method (ZD1).

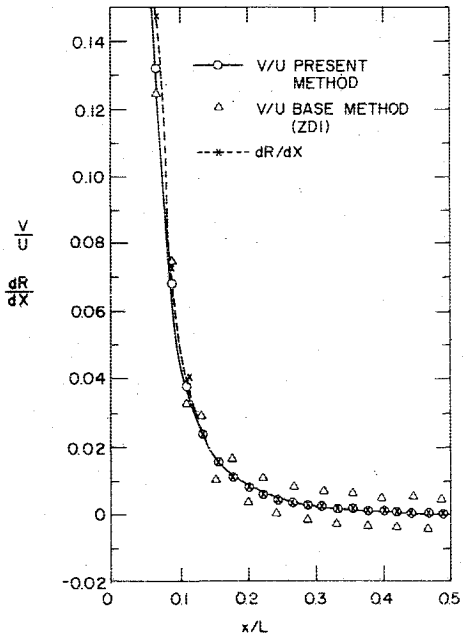

Fig. 11 A comparison between the ratio of the velocity components V/U (as calculated by the present inverse problem scheme and the base method ZD1) and the slope of the meridian line dR/dX.

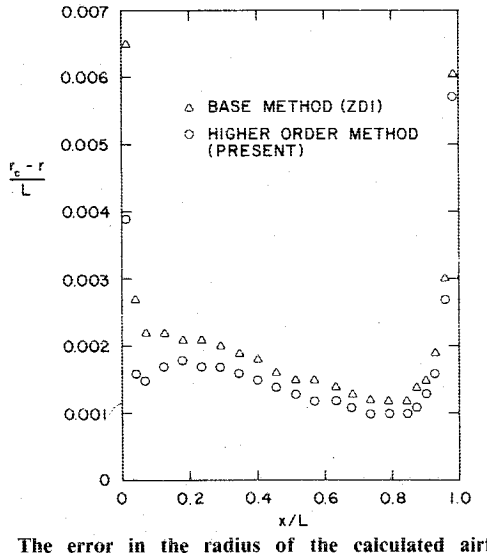

Fig. 12 The error in the radius of the calculated airfoil-type axisymmetric body of FR ≅ 2.91, $N = 36$.

FR ≅ 4.46

Comparison of the results of the base and the present methods, using 44 elements, shows that the trends presented for FR = 2.91 are generally still valid. Convergence was obtained after four iterations for both methods. The present method has slightly less error everywhere. Once again, we note that the accuracy of the present method was affected very slightly by the use of single precision calculations as compared to the base method.

Test Case 3: Low Drag Laminar Profile[18]

The velocity distribution given in Ref. 18 for this shape was input to the inverse problem program. The program stopped in the first iteration to calculate the body shape because of a negative value for R^2 corresponding to a point just after the inflection point. Then we closed the body tail by increasing the body length by 3% and calculated the velocity distribution for this slightly modified body by the present direct problem scheme. This calculated velocity distribution was then input to the inverse problem program. The program performed normally, and convergence was attained in three iterations. A comparison between the converged geometry and the correct one is shown in Fig. 13. Good agreement is obtained over about 70% of the body length, while the error in the rear 30% is small but not negligible. We recognize that changing the tailboom shape can change the aft pressure distribution. However, we felt that calculations on this body shape were important to demonstrate the method. This example demonstrates that the method may need further refinement to deal with a tailboom shape with an inflection point. This work is currently being undertaken.

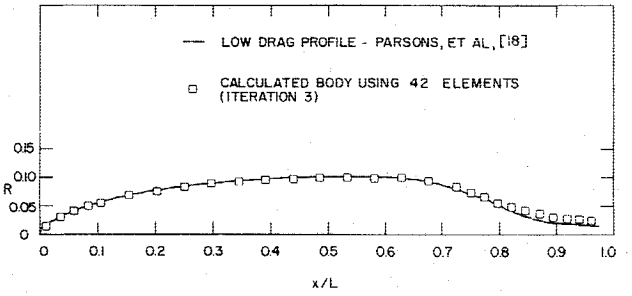

Fig. 13 Comparison between calculated and exact low-drag body shapes.

VI. Conclusions

The use of a linear variation of source strength over an element length has been demonstrated to improve the computational capability for flow over bodies of revolution. The present method for the direct problem produced results for standard body shapes that are substantially more accurate than the von Kármán method, even though computing time and storage requirements are about the same. One of the most important features of the present method is its ability to deal with bodies having an inflection point in the meridian contour. Agreement with the surface singularity method was very good at all points (except one), while the von Kármán method produced incorrect velocities in the rear portion of the body. Moreover, the present method proved to be more stable and much less sensitive to both the number of elements and the body length. While double-precision calculations were necessary for the von Kármán method, the present method produced stable and accurate results with single precision (8-digit accuracy). The direct method required 15000 words of storage for a maximum of 40 elements, within the bounds of a microcomputer. A typical case (20 elements) required 4 seconds of CPU time (including compilation, collection and execution). The actual computation time was 0.5 second. The computer used was the Univac 1108.

We think that, for application within the range of test cases presented here, the present method provides a simple and efficient alternative to the sophisticated, and more numerically involved, surface singularity method without significant sacrifice of accuracy. However, we recognize that the present method is incapable of the solving the flow around bodies with sharp corners or sudden changes in slope. In such cases, the surface singularity method is the best alternative.

The inverse problem is also solved by representing the body by an axial singularity distribution with linearly varying strength over each element. An iterative procedure has been devised by using two equivalent conditions, namely the tangency condition and the constant stream function on the body surface. The approach is generally similar to ZD1. The two methods were applied to a number of test cases. The body geometry converged in four iterations for the two methods; however, results of the present method are more accurate, especially for low-fineness ratios. Compared to the iterative method based on the surface-singularity distribution which has been developed by Bristow, the speed of convergence of

the present method is impressive. While ten iterations were necessary to obtain the excellent results presented by Bristow, the present method converged in four iterations and with a much simpler computational procedure in each iteration. However, our method cannot deal with the design of body shapes with sharp corners or sudden changes in slope. The inverse method required 17,000 words of storage for a maximum of 44 elements, also within the storage bounds of a microcomputer. A typical case (36 elements) required 11.5 seconds of CPU time (includes compilation, collection, and execution). The actual computation time was 6.8 seconds. Again, the computer used was the Univac 1108.

References

[1] Hess, J. L. and Smith, A. M. O., "Calculation of Potential Flow About Arbitrary Bodies," *Progress in Aeronautical Sciences*, Vol. 8, Pergamon Press, New York, 1967.

[2] von Kármán, T., "Calculation of the Flowfield Around Airships," NACA TM 574, July 1930.

[3] Oberkampf, W. L., and Watson, L. E., "Incompressible Potential Flow Solutions for Arbitrary Bodies of Revolution," *AIAA Journal*, Vol. 12, March 1974, pp. 409-411.

[4] Karamcheti, K., *Principles of Ideal-Fluid Aerodynamics*, Wiley & Sons, New York, 1966.

[5] Smith, A. M. O., and Pierce, J., "Exact Solution of the Neumann Problem," Douglas Aircraft Co., Long Beach, Calif., Douglas Rept. ES 26988, April 1958.

[6] Hess, J. L., "The Problem of Three-Dimensional Lifting Potential Flow and Its Solution by Means of Surface Singularity Distribution," *Comp. Meth. in Appl. Mech. & Engr.*, Vol. 4, 1974, p. 283.

[7] Hess, J. L., "Review of Integral-Equation Techniques for Solving Potential Flow Problems with Emphasis on the Surface-Source Method," *Comp. Meth. in Appl. Mech. & Engr.*, Vol. 5, 1975, p. 145.

[8] Webster, W. C., "The Flow About Arbitrary, Three-Dimensional Smooth Bodies," *Journal of Ship Research*, Vol. 19, 1975, p. 206.

[9] Grodtkjaer, E., "A Direct Integral Equation Method for the Potential Flow About Arbitrary Bodies," *International Journal for Numerical Methods in Engineering*, Vol. 6, 1973, p. 253.

[10] Hess, J. L., "On the Problem of Shaping an Axisymmetric Body to Obtain Low Drag at Large Reynolds Numbers," *Journal of Ship Research*, Vol. 20, 1976, p. 51.

[11] Young, A. D. and Owen, P. R., "A Simplified Theory for Streamlined Bodies of Revolution and its Application to the Development of High-Speed Low-Drag Shapes," British ARC R&M 2071, July 1943.

[12] McNown, J. S. and Hsu, E. Y., "Approximation of Axisymmetric Body Forms for Specified Pressure Distributions," *Journal of Applied Physics*, Vol. 22, 1951, p. 864.

[13] Marshall, F. J., "Design Problem in Hydrodynamics," *Journal of Hydronautics*, Vol. 4, Oct. 1970, pp. 136-139.

[14] Bristow, D. R., "A Solution to the Inverse Problem for Incompressible, Axisymmetric Potential Flow," AIAA Paper 74-520, June 1974.

[15] Zedan, M. F. and Dalton, C., "Incompressible, Irrotational, Axisymmetric Flow about a Body of Revolution; the Inverse Problem," *Journal of Hydronautics*, Vol. 12, Jan. 1978, pp. 41-46.

[16] Eskinazi, S., *Vector Mechanics of Fluids and Magnetofluids*, Academic Press, New York, 1967.

[17] Hamming, R. W., *Numerical Methods for Scientists and Engineers*, McGraw-Hill, New York, 1973.

[18] Parsons, J. S., Goodson, R. W., and Goldschmied, F. R., "Shaping of Axisymmetric Bodies for Minimum Drag in Incompressible Flow," *Journal of Hydronautics*, Vol. 8, July 1974, pp. 100-107.